SANDIA REPORT
SAND2005-7287
Unlimited Release
Printed November 2005

Rhombohedral AlPt Films Formed by Self-propagating, High Temperature Synthesis

David P. Adams, Mark A. Rodriguez and Paul G. Kotula

Prepared by
Sandia National Laboratories
Albuquerque, New Mexico 87185 and Livermore, California 94550

Sandia is a multiprogram laboratory operated by Sandia Corporation,
a Lockheed Martin Company, for the United States Department of Energy's
National Nuclear Security Administration under Contract DE-AC04-94AL85000.

Approved for public release; further dissemination unlimited.

Issued by Sandia National Laboratories, operated for the United States Department of Energy by Sandia Corporation.

NOTICE: This report was prepared as an account of work sponsored by an agency of the United States Government. Neither the United States Government, nor any agency thereof, nor any of their employees, nor any of their contractors, subcontractors, or their employees, make any warranty, express or implied, or assume any legal liability or responsibility for the accuracy, completeness, or usefulness of any information, apparatus, product, or process disclosed, or represent that its use would not infringe privately owned rights. Reference herein to any specific commercial product, process, or service by trade name, trademark, manufacturer, or otherwise, does not necessarily constitute or imply its endorsement, recommendation, or favoring by the United States Government, any agency thereof, or any of their contractors or subcontractors. The views and opinions expressed herein do not necessarily state or reflect those of the United States Government, any agency thereof, or any of their contractors.

Printed in the United States of America. This report has been reproduced directly from the best available copy.

Available to DOE and DOE contractors from
U.S. Department of Energy
Office of Scientific and Technical Information
P.O. Box 62
Oak Ridge, TN 37831

Telephone: (865) 576-8401
Facsimile: (865) 576-5728
E-Mail: reports@adonis.osti.gov
Online ordering: http://www.osti.gov/bridge

Available to the public from
U.S. Department of Commerce
National Technical Information Service
5285 Port Royal Rd.
Springfield, VA 22161

Telephone: (800) 553-6847
Facsimile: (703) 605-6900
E-Mail: orders@ntis.fedworld.gov
Online order: http://www.ntis.gov/help/ordermethods.asp?loc=7-4-0#online

SAND2005-7287
Unlimited Release
Printed November 2005

Rhombohedral AlPt Films Formed by Self-propagating, High Temperature Synthesis

David P. Adams, Mark A. Rodriguez and Paul G. Kotula
Thin Film, Vacuum& Packaging Department
Sandia National Laboratories,
P.O. Box 5800
Albuquerque, NM 87185-1245

ABSTRACT

High-purity AlPt thin films prepared by self-propagating, high temperature combustion synthesis show evidence for a new rhombohedral phase. Sputter deposited Al/Pt multilayers of various designs are reacted at different rates in air and in vacuum, and each form a new trigonal/hexagonal aluminide phase with unit cell parameters a = 15.571(8) Å, c = 5.304(1) Å, space group *R-3* (148), and Z, the number of formula units within a unit cell, = 39. The lattice is isostructural to that of the AlPd R-3 lattice as reported by Matkovic and Schubert (Matkovic, 1977). Reacted films have a random in-plane crystallographic texture, a modest out-of-plane (001) texture, and equiaxed grains with dimensions on the order of film thickness.

Keywords: AlPt, x-ray powder diffraction, Rietveld refinement, self-propagating high temperature synthesis, exothermic thin film

I. INTRODUCTION

The equilibrium phase formation and thermodynamics of the Al-Pt binary system have been investigated thoroughly in the past. McAlister and Kahan have completed an extensive review of previous experiments(McAlister, 1986); a phase diagram from their work is shown in Figure 1. Although some questions remain regarding $AlPt_2$ and the low temperature form of $AlPt_3$, the equilibrium phases of Al-Pt are well studied. Various intermetallics are identified in the phase diagram as summarized in Table 1. Of interest to current work, there are two reported solid phases having a stoichiometry of ~1:1. This includes an equilibrium phase AlPt having a cubic FeSi-type structure and Pearson symbol *cP*8 (Ferro, 1963; Schubert, 1956). Studies confirm that this phase has nil solubility about 50 atomic % Pt; at this composition the liquidus is 1554°C. A high-temperature β phase isomorphous with NiAl has also been reported to be stable above 1260°C.(Bhan, 1978; Chattopadhyay, 1975) The β phase forms across a limited compositional range from ~52 to ~56 at. % Pt. There are a number of Al-rich and Pt-rich phases. Off a ~1:1 stoichiometry, phases include: a cubic $Al_{21}Pt_5$ phase with nil solubility, a tetragonal $Al_{21}Pt_8$ phase with nil solubility, a cubic Al_2Pt phase with a solubility of ~ 1 at. %, a hexagonal Al_3Pt_2 phase with nil solubility, an orthorhombic Al_3Pt_5 phase with a solubility range of 1 to 2 at. %, an orthorhombic $AlPt_2$ phase having a solubility range of 1 to 2 at. %, and a cubic $AlPt_3$ with a solubility range of ~ 10 at. %.

In this document we describe a new phase for AlPt that indexes as rhombohedral similar to that of rhombohedral AlPd as presented by Matkovic and Schubert (Matkovic, 1977). We emphasize that no equilibrium or metastable phases reported in the literature exhibit this same structure. Rhombohedral AlPt is formed by rapid, high-temperature combustion of sputter-deposited, high-purity Al/Pt nanolaminates. Self-propagating, high temperature synthesis is generally regarded as a nonequilibrium process.

II. EXPERIMENTAL PROCEDURES

Thin film deposition*:*

Al/Pt multilayer coatings are first deposited by sputter deposition and then reacted to form AlPt. Multilayers consist of alternating films of high purity Al and Pt grown by Ar sputter deposition in a cryopumped, ultra-high vacuum chamber (base pressure = $8x10^{-8}$ Torr; Unifilm, Co.). High purity Al (99.9995%) and Pt (99.95%) targets are used for

growth with each presputtered for ~15 minutes prior to the start of multilayer deposition. We use ultra-high purity Ar (99.995%) for all sputter processes.

Films are deposited onto clean Si(100) substrates having a 4000 Å thick thermal oxide (Silicon Sense, Inc.). The thermal oxide layer is chosen so to prevent reaction of metal with silicon during deposition and during high temperature combustion. Note, although substrates did not exceed 60°C during deposition, transmission electron microscopy shows an 80 Å thick, amorphous Al_xPt_y layer at each interface within the multilayer. This presumably occurs because of interdiffusion at the growth temperature, and mixing resulting from energetic beam bombardment. Sputter deposition is automated through sample/stage translation and rotation so to precisely control individual layer thickness and minimize transit time (~5 sec) between metal targets. Quartz crystal monitors are used to monitor film thickness with Angstrom level precision. Thickness calibrations are conducted immediately prior to deposition using a DEKTAK surface profilometer and checked by cross-section transmission electron microscopy.

All multilayers are designed to have equal parts Al and Pt. Individual layer thicknesses (from 100 – 1000 Å) were adjusted to compensate for the different Al and Pt film densities. We use measured thin film densities determined by independent x-ray reflectivity measurements when designing multilayers. Multilayer films are deposited to total thicknesses ranging from 0.25 – 2.4 μm with the thickness of individual Al and Pt layers fixed for a given multilayer. We have confirmed that as-deposited Al and Pt layers are high purity. Depth profiling Auger electron spectroscopy analysis of Au-capped Al layers shows < 0.5 at. % O in Al while similar analysis of Au-capped Pt layers indicates no impurities within the bulk of sputtered Pt.

X-ray Diffraction (XRD) Specimen Preparation:

Reacted film specimens are mounted on a small stub of amorphous epoxy within a deep-well, glass holder for XRD. Samples are pressed down to be level with the edge of the fixture in order to minimize effects of specimen displacement during analysis. To reduce background, care is taken to avoid exposure of the epoxy. AlPt films deposited on an oxidized Si substrate are of sufficient size to encompass the entire beam footprint over the 2θ range scanned.

XRD Data Collection:

A Siemens D500 θ–2θ powder diffractometer is used for data collection with samples maintained at room temperature. The data are collected over a scan range of 10-65° 2θ at a step size of 0.04^o 2θ and a dwell-time of 20 sec. Additional peaks are observed at larger 2θ angles, however due to the large intensity of the Si (400) reflection near 69° 2θ, the maximum scan range is limited to 65° 2θ. Monochromatic Cu Kα (0.15406nm) radiation is produced using a diffracted beam curved graphite monochrometer. Fixed slits of 1.0, 1.0, 1.0, 0.15, & 0.15 degrees are used, and the instrument power settings are 45kV and 30mA. Alignment and calibration are checked using a LaB_6 (NIST SRM660) external standard. Datascan V3.1 (Materials Data Inc.) software is used to operate the diffractometer.

III. RESULTS AND DISCUSSION

Combustion synthesis and purity of reacted layers

As depicted in Figure 2, self-propagating high-temperature reactions are used to transform high-purity, vapor deposited Al/Pt multilayers into AlPt. Self-propagating reactions have previously been used for combustion synthesis of many alloys and compounds including carbides, oxides, nitrides, borides and various intermetallics.(Moore, 1995) A local reaction is triggered by an external stimulus (e.g., laser, electrical discharge, etc.) leading to the mixing of a volume of neighboring reactant layers. The combination of Al and Pt gives off heat thus raising the temperature in surrounding volumes of multilayer further promoting mixing in adjacent areas. A self-propagating process continues laterally through the entire nanometer-scale laminate until all reactant layers are consumed.(Barbee, 1996) A self-propagating, high temperature reaction is to be expected for this material pair based on the high heat of reaction, a large adiabatic reaction temperature, and the low melting point of Al. The Al – Pt system is characterized by large heats of formation as listed in Table 1. For a 1:1 stoichiometry ΔH_f is determined by experiment to be -100 kJ/mol of atoms at 25 ^{o}C (De Boer, 1988). Fischer and Grubelich have reported a large adiabatic reaction temperature, $T_{ad,}$ equal to

2800°C.(Fischer, 1998) Because thin AlPt films remain attached to nonenergetic oxidized Si substrates through synthesis, we expect reaction under non-adiabatic conditions and combustion temperatures substantially below T_{ad}.

Films having different multilayer designs have been fabricated and tested to determine the rate of reaction. Figure 3 shows evidence of a self-propagating reaction ignited by an electronic match. This particular film is shown to react in plan view with a characteristic uniform steady-state propagation speed. Unreacted multilayer is recognized as a relatively bright layer with the alloy having a darker appearance due to a larger surface roughness. High-speed photography of films such as that shown in Figure 3 demonstrate velocities ranging from 20 – 90 m/s depending on multilayer design. Consistent with previous work by Barbee and Weihs (Barbee, 1996), the velocity is found to increase with decreasing bilayer thickness for a range of multilayer designs. This has been explained to occur because the relevant diffusion lengths are reduced when constructing multilayers of small bilayer thickness. Considered a mass transport limited process, films react with higher speed as the reactants are positioned in closer proximity. Figure 4 summarizes speeds measured from films of different bilayer and total thickness.

Films reacted in air and in vacuum are analyzed for purity by depth-profiling Auger electron spectroscopy (AES). This surface analysis technique shows that reacted films are pure within their bulk. Depth-profile analysis shows a thin oxide (~ 0.06 μm) on the surface of foils reacted in air but no evidence for oxygen in the bulk of films. The small amount of impurities in the near-surface region of films reacted in air is likely due to the high reaction speed of films. AES also confirms a constant AlPt stoichiometry through the thickness of reacted foils for all designs considered. A uniform mixture of high purity Al and Pt shown by AES is consistent with studies of film structure formed through slow annealing. As predicted by an equilibrium phase diagram AlPt of 50 at. % is expected to form an FeSi-type structure (of nil solubility) given sufficient time. We have taken as-deposited Al/Pt thin film multilayers grown onto single crystal sapphire substrates and annealed them for structural analysis by x-ray diffraction. Consistent with multilayer designs having equal parts Al and Pt, an FeSi-type structure is found to develop at temperatures ~ 650 ^{o}C. The θ–2θ diffraction pattern shown in Figure 5 is of an annealed AlPt film; it clearly shows the presence of peaks associated with an FeSi-

type lattice. Also shown in this figure is the simulated x-ray powder diffraction pattern of AlPt (FeSi-type structure) for comparison. The *'s in the figure indicate extra peaks from a confirmed thin interfacial phase resulting from reaction with the substrate.

Structural analysis of reacted foils

Figure 6 displays the powder diffraction pattern obtained for AlPt formed by self-propagating high temperature synthesis along with a simulated pattern of the rhombohedral AlPd taken from Matkovic and Schubert (Matkovic, 1977). As one can see, the AlPt pattern is very similar to the AlPd, with only minor variations in peak position and intensity. X-ray powder diffraction data for rhombohedral AlPt are given in Table 2. To generate a powder diffraction file (PDF) entry (ICDD, 2006) for rhombohedral AlPt the reflections are fit using the least-squares refinement program within the JADE v.7.1 (Materials Data, Inc.) software package. Attempts are made to fit overlapped reflections. This is met with minor success and several peaks must be fit as single profiles even though it is clear from the predicted cell that there are multiple hkℓ's present within the peak profile. Peaks with multiple hkℓ contributions are labeled with a (+) symbol next to the assigned hkℓ to indicate additional intensity contribution from an overlapping reflection. This difficulty in separating peak profiles results in part from the rather large unit cell, which generates a large number of possible hkℓ values. This is additionally confounded by the presence of micro-strain within the film, resulting in large peak full-widths that increased with 2θ. Micro-strain is to be expected based on the quenching of a film adhered to a substrate following synthesis. Based on these observations, the powder diffraction data are optimized to make use of as many peak profiles as possible, while still obtaining a reasonable refinement of the unit cell. Weak reflections caused particular problems with pattern refinement. Although some of these very weak (< 1% I/Io) reflections could be detected [e.g. the overlapped (342)/(630) doublet at d ~ 1.70 Å (~53.9^{o} 2θ)] it is not possible to obtain good profile-fit results with reasonable FWHM or reliable peak location values for small peaks. For this reason, reflections having < 1% relative intensity are not reported in the PDF pattern. An additional difficulty manifest in the refinement when the 2nd most intense peak, the (131)

reflection at d ~ 3.04 Å ($2\theta = 29.3^o$), displayed a 2θ error of more than 0.15^o. Due to this fact, additional indexation attempts are made to determine if another cell would be more appropriate. Multiple attempts at indexation repeatedly generated the R-3 cell as the best fit to the data, even with the large error associated with the (131) peak. The two most likely reasons for this large shift are anisotropic macro-strain or the presence of a second phase, with the former being the most likely candidate. In reviewing Table 2, it is notable that several other $hk\ell$'s show deviations larger than 0.05^o 2θ, namely the (321), (042), and (003)+ peaks. It is easy to explain these deviations because the (321) and (042) peaks have very low intensity and (003)+ overlaps the (621) reflection but could not be refined as two independent profiles. Although inadequate profile-fitting could be the culprit for such deviations, it is also possible that strain plays a major role in the 2θ deviations observed. What clearly stood out from the refinement process was that removal of the (131) peak dramatically improved the lattice parameters in terms of standard error values and $\Delta 2\theta$. The Smith and Snyder (Smith, 1979) figure of merit for the refinement with the removal of the (131) peak was $F_{18} = 14.2$ with a $|2\theta| = 0.025^o$ for 51 possible reflections. These refinement results, while adequate, are not remarkably impressive. In this instance it is useful to compare these results to that of the rhombohedral AlPd structure (PDF # 00-042-0766) which reported an $F_{30} = 18.1$ with a $|2\theta| = 0.044^o$ for 38 possible reflections. In this context the refinement of the AlPt diffraction data seems quite respectable considering the difficulties inherent to the refinement of this structure type.

Rietveld crystal structure refinement for rhombohedral AlPt is carried out using GSAS.(Larson, 2000) Initial unit cell parameters are obtained from the lattice parameter refinement. Conditions for the refinement are listed in Table 3. A total of 22 parameters including 15 structural parameters are refined. The atomic scattering factors for Al and Pt are taken from the International Table for X-ray Crystallography IV (1974). Figure 7 shows the quality of fit for the refinement when the (131) peak is present and absent. There is a dramatic reduction in the pattern residual error, R_p, value from 26.5% to 17.7% when the (131) reflection is removed from the refinement. As discussed earlier for the lattice parameter refinement, it is not clear why this discrepancy occurs for the (131)

reflection, but like the powder diffraction data, the structure refinement benefits from the removal of this hkℓ. Also note in Table 3 that there is an apparent out-of-plane preferred orientation for the (00ℓ) as noted by the March-Dollase preferred orientation parameter with that refined to 0.78(1). This value indicates a modest preference for the c-axis to orient out-of-plane. This type of orientation is not unexpected for a rhombohedral/hexagonal system, and the texture is not severe as to limit observation of major reflections. Crystal data for both the least-squares refinement and the Rietveld refinement are shown in Table 4 for comparison purposes. Unit cell parameters obtained using the least-squares refinement method are in good agreement with those obtained in the Rietveld refinement. Atom fractional coordinates and site occupancies for the Rietveld refinement of rhombohedral AlPt are given in Tables 5. Refinement of the Al atom positions proved difficult, with large deviations in fraction coordinates during the refinement process. This resulted in Al positions that generated unrealistically short bond lengths. It was found that when the Al atoms were set and fixed to the reported fractional coordinates reported for AlPd and only the heavier Pt atoms were allowed to refine, the structure refinement was stable with reasonable bond lengths being generated. Attempts were made to refine the site occupancies for the Al and Pt atoms. All the sites refined to within 5% of full occupancy and therefore were fixed for the final refinement and reported as fully occupied. To obtain a measure of the deviation away from refined site positions, an overall atomic displacement parameter, *Biso*, was refined as reported in Table 3. This value tended to be elevated. The lack of an infinitely thick specimen is likely to be the source of this deviation. For an incident beam angle of 15° 2θ and an AlPt film thickness of 1 μm, roughly 97% of the intensity would come from the film with the balance penetrating into the substrate. This value is reduced to 65% for 65° 2θ. The net result is that the overall temperature parameter can become elevated as it attempts to compensate for this intensity variability. This intensity deviation should be kept in mind when considering the relative intensities of the reported hkℓ's listed in table 2. Specifically, peaks at higher 2θ values will have reduced relative intensities as compared to infinitely thick specimens. Because this sample could not be produced as a bulk powder, it was not possible to collect optimum diffraction data. Clearly the beam

penetrates through the film and into the Si substrate because the Si (400) peak was observed in the diffraction data. There also is an additional artifact in the data confirming the beam penetration. If one looks closely, one can observe a $\lambda/2$ peak for the Si (400) at ~33° 2θ. This small artifact is typical and does not significantly affect the outcome of the refinement results. The cell volume reported for AlPd was 1115 Å^{3}. This is essentially the same unit cell volume obtained for AlPt as shown in Table 4. There is a small difference in lattice parameters observed for the two isostructural compounds. The AlPd structure reported lattice parameters of a = 15.659 Å and c = 5.251 Å. These are similar to the refined values reported in Table 4 for AlPt (a = 15.576 Å and c = 5.306 Å). This shows a -0.083 Å shrinkage of the a axis and +0.055 Å expansion of the c axis for AlPt as compared to the AlPd cell.

IV. SUMMARY

With regard to the combustion synthesis of Al/Pt multilayer thin films we find the following:

1. Multilayer Al/Pt thin films exhibit high-temperature, self-propagating reactions when chemically bonded to silicon dioxide substrates.
2. Reaction speeds vary from 20-90 m/s with multilayer design according to bilayer thickness and total thickness selected.
3. High purity AlPt thin films with 1:1 stoichiometry form as a result of self-propagating reactions
4. a newly-discovered rhombohedral phase of AlPt is generated during this process.
5. The rhombohedral phase of AlPt has unit cell parameters a = 15.571(8) Å, c = 5.304(1) Å, and a space group *R-3* (148).
6. The rhombohedral AlPt phase is isostructural with a previously-reported phase of AlPd.
7. Reacted films have a random in-plane crystallographic texture, a modest out-of-plane (001) texture, and equiaxed grains with dimensions on the order of film thickness.

V. ACKNOWLEDGEMENTS

The authors gratefully acknowledge the work of J. Sobczak and K. Archuleta for thin film deposition, R. Wayne Buttry for AES, M. Rye for sample preparation and D. Wackerbarth for high-speed photography. The United States Department of Energy supported this work under Contract DE-AC04-94AL85000. Sandia is a multi-program laboratory operated by Sandia Corporation, a Lockheed Martin Company, for the United States Department of Energy.

VI. REFERENCES

Barbee Jr., T.W. and Weihs, *Ignitable Heterogeneous Stratified Structure for the Propagation of an Internal Exothermic Chemical Reaction along an Expanding Wavefront and Method of Making Same*, T., United States Patent # 5,538,795. Jul. 23, 1996.

Bhan, S. and Kudielka, H. (1978) Z. Metallkd., **69**, 333-334.

Chattopadhyay, T. and Schubert, K. (1975) J. Less Common Met., **41**, 19-32.

De Boer, F.R., Boom, R., Mattens, W.C.M, Miedema, A.R., and Niessen, A.K., in Cohesion in Metals: Transition Metal Alloys (North Holland, Amsterdam, 1988).

Dollase, W. A. (1986), J. Appl. Crystallogr. **19**, 267-272.

Ellner, M., Kattner, U. and Predel, B. (1982) J. Less-Common Met., **87**, 305-325.

Ferro, R., Capelli, R. and Rambaldi, G. (1963) Atti Accad.Naz. Lincei, Rend. Classe Sci. Fis. Mat. Nat. **34**, 45-47. (in German)

Fischer, S.H. and Grubelich, M. C. (1998) Sandia National Laboratories, SAND Report 98-1176C.

Huch, R. and Klemm, W., (1964) Z. Anorg. Chem. **329**,123-135.

ICDD, International Centre for Diffraction Data, (2006) Newtown Square, PA. PDF entry for AlPt powder diffraction data (to be submitted).

International Tables for X-ray Crystallography (1974). Vol. IV. (Kluwer Academic, Boston), pp. 71.

Jenkins, R., and Snyder, R. L. (1996), *Introduction to X-Ray Powder Diffractometry* (Wiley, New York), pp.149-150.

Larson, A.C. and Von Dreele, R.B., "General Structure Analysis System (GSAS)", Los Alamos National Laboratory Report LAUR 86-748 (2000).

March, A. (1932). Z. Kristallogr., **81**, 285-297.

Matkovic, T. and Schubert, K., (1977). J. Less Common Met., **55**, pp. 45-52.

McAlister, A.J. and Kahan, D. J., (1986). “The Al-Pt (Aluminum-Platinum) System,” *Bulletin of Alloy Phase Diagrams*, **7**, pp. 47-51.

Moore, J.J., and Feng H.J., (1995) Progress in Mat. Sci. 39, 243-273.

Oyo, Y., Mishima, Y. and Suzuki, T., (1987) Z. Metallktd., **78**, 485-490.

Piatti, G. and Pellegrini, G., (1980) J. Mater. Sci., **15**, 2403-2408.

Pretorius et. al. J. Appl. Phys. (1991) 70, 3636.

Saalfeld, Von H. (1973). "Crystallographic Investigations of Glaserite from Mount Vesuvius (Italy)," Neues Jahrb. Mineral. **2**, 75-78

Schubert, K., Burkhardt, W., Esslinger, P., Gunzel, E., Meissner, H., Schutt, W., Wegst, J., and Wilkens, M. (1956) Naturwissenschaften, **43**, 248-249 (in German).

Schwarz, Von H. (1966). " I. Sulfate," Z. Anorg. Allg. Chem. **344**, 41-55

Smith, G. S. and Snyder, R. L. (1979). "F(N): A Criterion for Rating Powder Diffraction Patterns and Evaluating the Reliability of Powder Pattern Indexing," J. Appl. Crystallogr. **12**, 60-65.

Wu, K. and Jin, Z., (2000). "Thermodynamic Assessment of the Al-Pt Binary System," *J. Phase Equilibria*, 21, pp. 221-226.

TABLE 1. Summary of intermetallic phases previously reported for the Al-Pt system. From McAlister (1986), Wu (2000).

Phase	Range (at.%Pt)	Pearson symbol	Space Group	Prototype	Lattice Parameters (nm) a	b	c	Reference	Enthalpy of Formation, kJ/mol of atoms
Equilibrium									
$Al_{21}Pt_5$	19.2	*Cubic*	-	-	1.932			1980 G. Piatti	-57 †
$Al_{21}Pt_8$	27.0	*tI116*	$I4_1a$	-	1.296		1.068	1982 M. Ellner	-71†
Al_2Pt	31.5 to 33.5	*cF12*	*Fm3m*	CaF_2	0.591			1982 M. Ellner	-84 †
Al_3Pt_2	40.0	*hP5*	*P3m1*	-	0.420		0.517	1963 R. Ferro	-95 †
AlPt	50.0	*cP8*	$P2_13$	FeSi	0.486			1956 K. Schubert	-100 †
β-AlPt(HT)	~52 to ~56	*cP2*	*Pm3m*	CsCl				1978 S. Bhan 1975 T. Chattopadhyay	
Al_3Pt_5	~61.5 to 63.0	*oP16*	*Pbam*	Ge_3Rh	0.541	1.070	0.395		-72*
$AlPt_2$	~66 to ~66	*oP12*	*Pnma*	$PbCl_2$					-88 †
$AlPt_2$ (LT)	~66 to ~67	*oP24*	*Pmma*	$GaPt_2$(LT)					-88 †
$AlPt_3$	~67.3 to ~77.7	*cP4*	*Pm3m*	$AuCu_3$	0.387			1964 R. Huch	
$AlPt_3$(LT)	~73.5 to 100	*tP16*	*P4/mbm*	U_3Si; $GaPt_3$(LT)				1987 Y. Oya, et. al.	-70 †
Metastable									
Al_4Pt	~ 20								-57 (-44)
Al_6Pt	~ 14								
ε’									
λ’	10 to 25								

† from Pretorius (1991).
* from De Boer (1988).

TABLE 2. X-ray powder diffraction data for rhombohedral AlPt. Radiation: Cu Kα_1 (0.15406 nm)

HKL	2θ CALCULATED (°)	2θ OBSERVED (°)	Δ2θ (°)	D-SPACING OBSERVED (Å)	I/IO
101	17.955	17.956	-0.001	4.9360	1.6
211	24.197	24.209	-0.013	3.6733	33.7
131	29.192	29.350	-0.158*	3.0406	62.0
410	30.349	30.341	0.009	2.9436	1.4
401	31.415	31.407	0.008	2.8460	3.4
321	33.505	33.561	-0.056	2.6681	2.3
012(+)	34.436	34.440	-0.004	2.6020	2.1
122	38.223	38.237	-0.015	2.3519	17.3
241	39.185	39.146	0.040	2.2994	8.3
511	40.928	40.929	0.000	2.2032	6.9
312(+)	41.716	41.716	0.000	2.1634	100.0
042	43.375	43.474	-0.100	2.0799	1.4
232	44.984	44.967	0.017	2.0143	1.3
422(+)	49.566	49.610	-0.044	1.8361	7.3
710(+)	51.094	51.083	0.012	1.7866	5.1
003(+)	51.655	51.579	0.076	1.7705	11.5
532(+)	59.234	59.248	-0.014	1.5583	1.0
811	61.220	61.181	0.039	1.5137	4.0
461	62.492	62.491	0.001	1.4850	3.3

* not used in cell refinement

TABLE 3. Experimental Conditions for Rietveld refinement of rhombohedral AlPt

formula weight	8659.2
2θ range for Rietveld refinement (° 2θ)	10 - 65
number of reflections in the 2θ range	190
March-Dollase preferred orientation factor along (00ℓ)	0.78(1)
overall atomic displacement parameter B_{iso}, (Å^2)	4.1(4)
Peak shape function	Pseudo-Voigt, (3 parameters)
Background function	Complex polynomial, n=3
Temperature (°C)	25
R_p	0.1769
R_{wp}	0.2215
R_e	0.0485

TABLE 4. Crystal structure data for rhombohedral AlPt

Crystal System	Trigonal/Hexagonal	
Space Group	R –3 (#148)	
Formula number in unit cell	Z = 39	
	Least Squares method	Rietveld method
a axis (Å)	15.571(8)	15.576(2)
c axis (Å)	5.304(1)	5.306(1)
Unit cell volume (Å^3)	1114(1)	1115(1)
D_x (g/cm^3)	12.9(1)	12.9(1)

TABLE 5. Positional Parameters for rhombohedral AlPt

Atom	x	y	z	Occupancy
Al(1)	0	0	0.5	1
Al(2)	0.1799	0.1117	0.1657	1
Al(3)	0.3200	0.0829	0.8365	1
Pt(1)	0	0	0	1
Pt(2)	0.1774(5)	0.1032(6)	0.674(1)	1
Pt(3)	0.3272(7)	0.0854(6)	0.328(1)	1

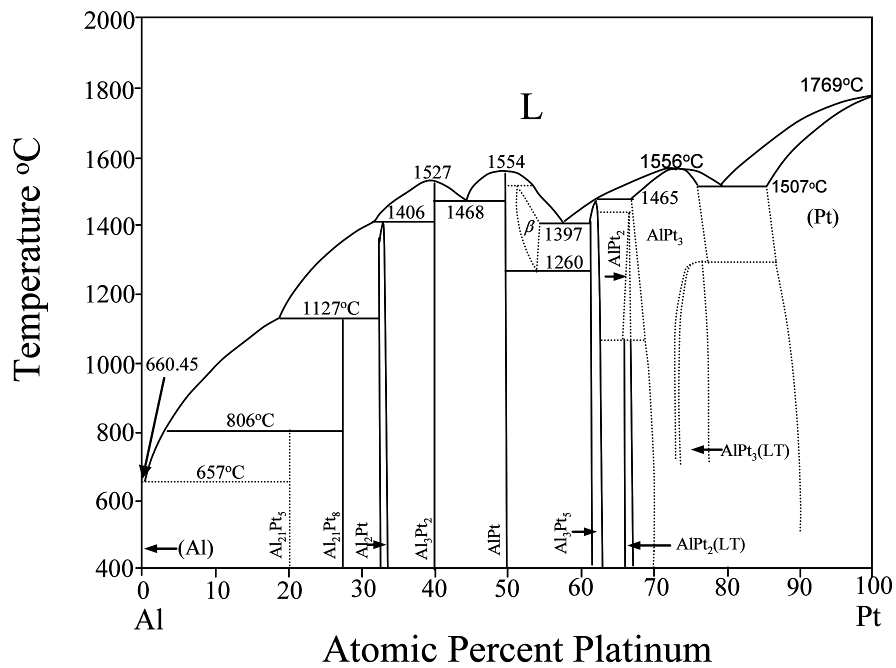

FIGURE 1. Equilibrium phase diagram of the Al-Pt system. (from McAlister and Kahan (1986).

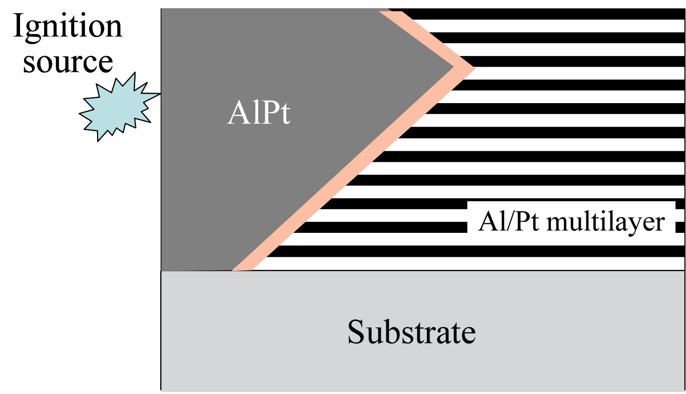

FIGURE 2. Illustration of self-propagating, high temperature synthesis of Al/Pt thin film multilayers.

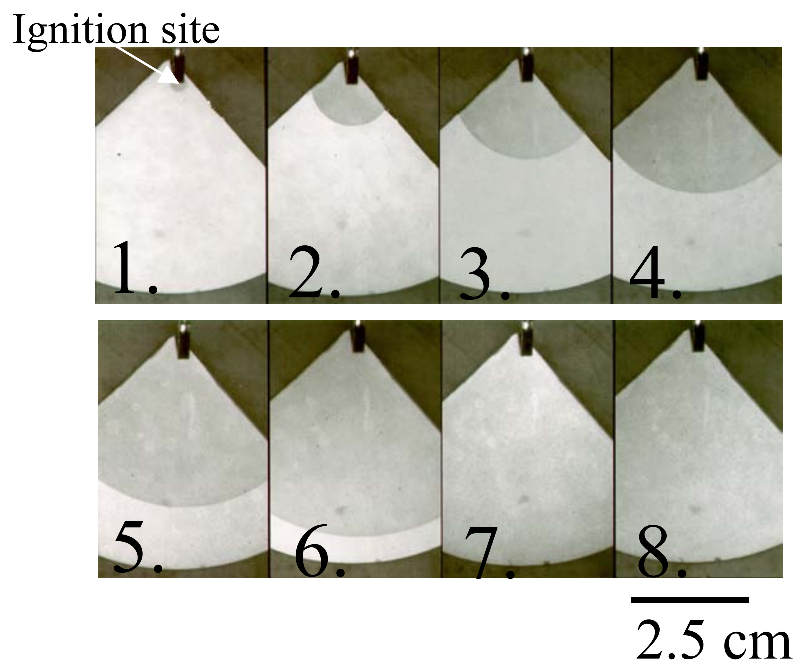

FIGURE 3. High-speed photography showing self-propagating high temperature reaction in Al/Pt multilayer thin films.

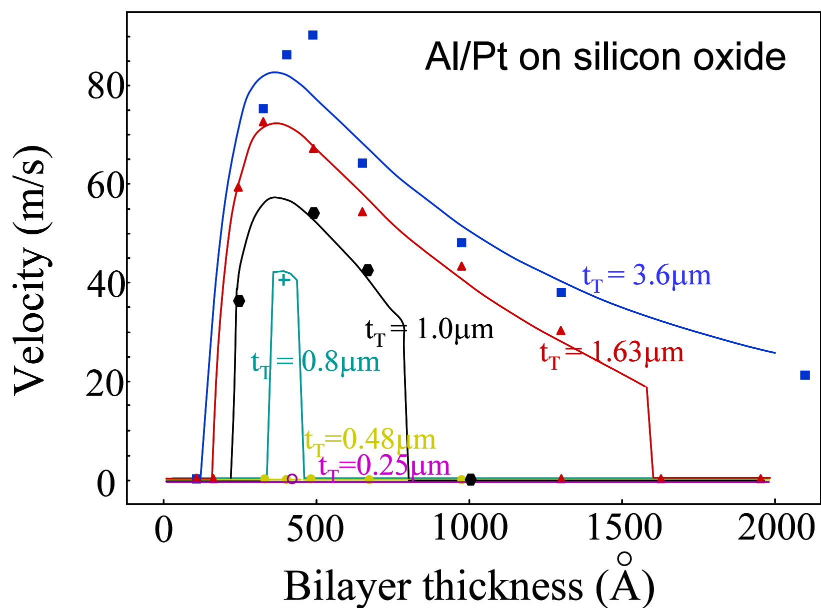

FIGURE 4 Plots of steady-state reaction velocity measured by high–speed photography versus bilayer thickness (i.e., 1 Al + 1 Pt layer). Films of different total thickness, t_T, are described.

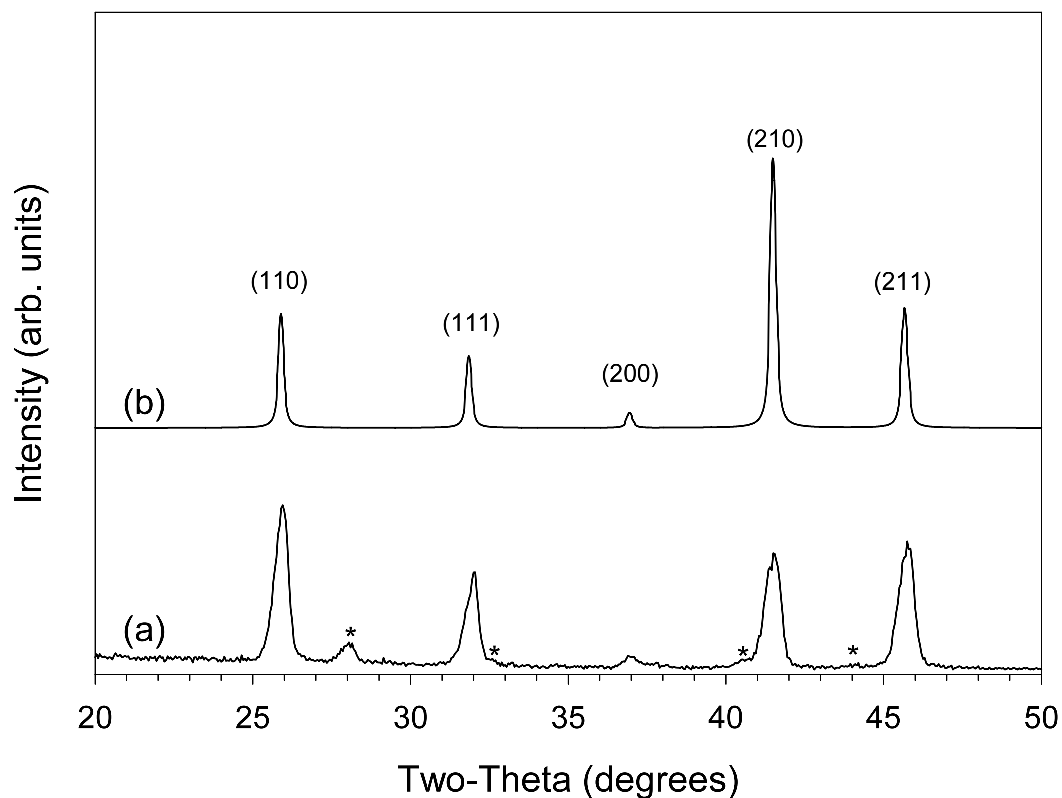

Figure 5. X-ray diffraction of an annealed AlPt multilayer showing evidence of a FeSi-type structure. (a) θ–2θ x-ray diffraction pattern of annealed AlPt film; *'s indicate extra peaks from a thin interfacial phase resulting from reaction with the substrate (confirmed by cross section TEM). (b) Simulated x-ray powder diffraction pattern for AlPt (FeSi-type structure).

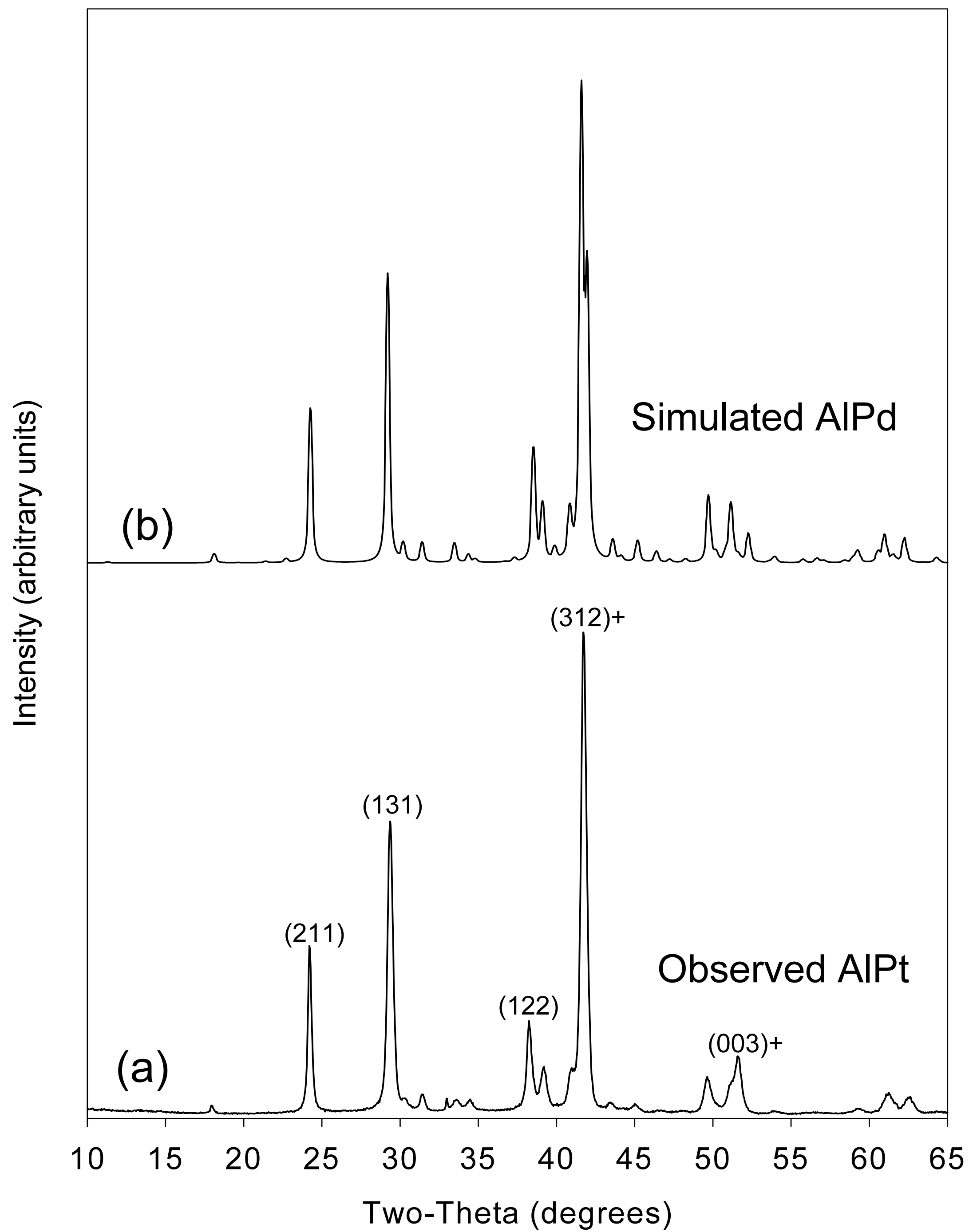

FIGURE 6. Comparison of (a) x-ray diffraction pattern taken from SHS-reacted AlPt thin films, and (b) simulated rhombohedral AlPd pattern.

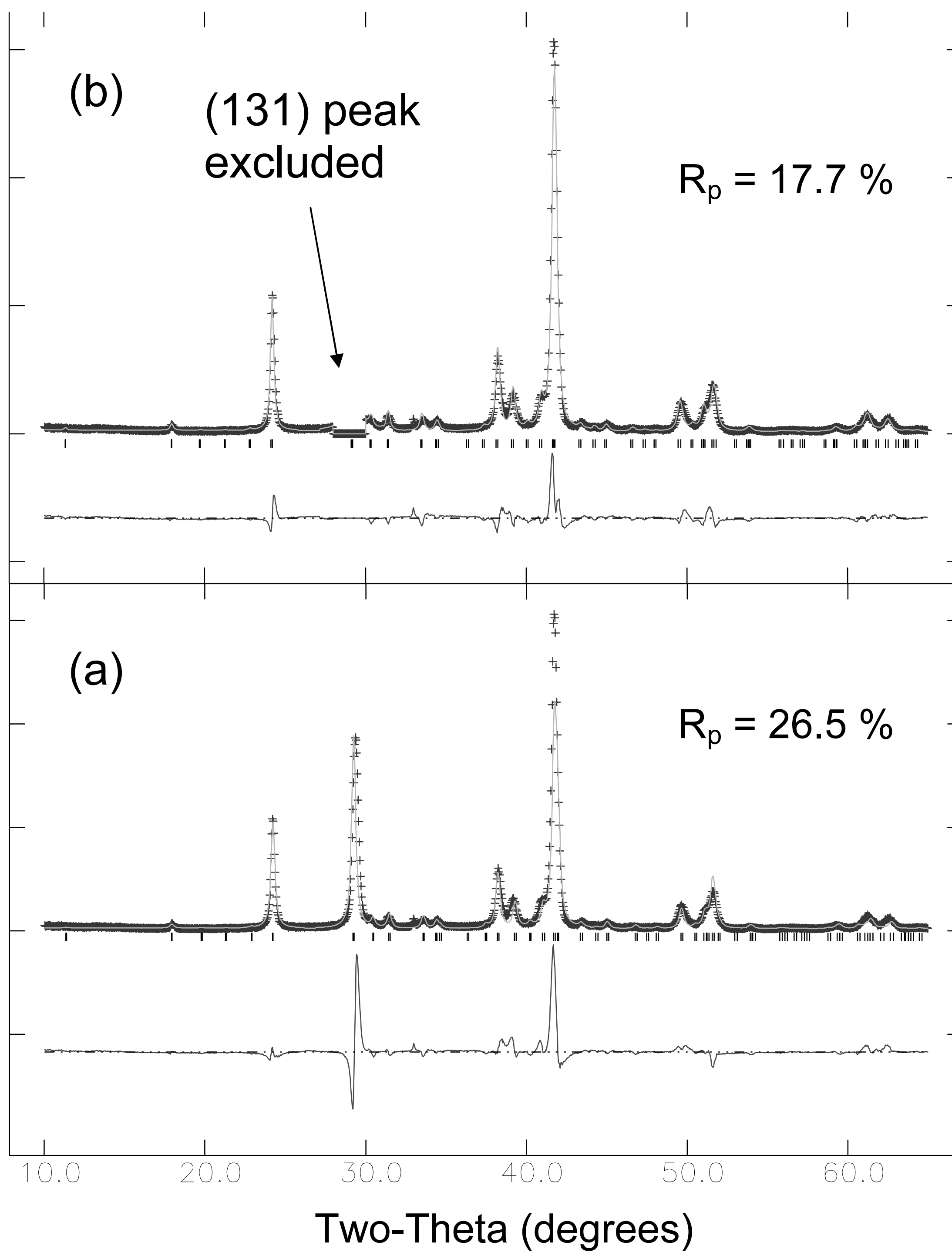

FIGURE 7. Structure refinement results for AlPt. (a) Rietveld refinement including (131) peak. (b) Rietveld refinement with removal of (131) peak.

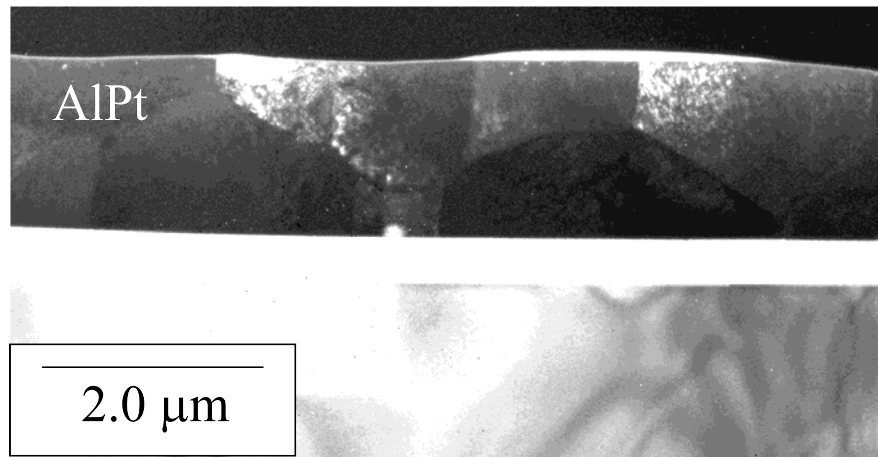

FIGURE 8 Cross-section, dark field transmission electron micrograph of AlPt reacted by high temperature synthesis.

Distribution list:

3	MS 1245	David P. Adams
1	MS 1411	Mark Rodriguez
1	MS 0886	Paul Kotula
1	MS 0959	Robert Poole
2	MS 0899	Technical Library
2	MS 9018	Central Technical Files
1	MS 0123	LDRD office